Biochimica et Biophysica Acta 1838 (2014) 1169–1179

Contents lists available at ScienceDirect

Biochimica et Biophysica Acta

journal homepage: www.elsevier.com/locate/bbamem

Plasticity and conformational equilibria of influenza fusion peptides in model lipid bilayers ☆

Neil R. Haria [a], Luca Monticelli [b], Franca Fraternali [c,*], Christian D. Lorenz [a,*]

[a] Theory and Simulation of Condensed Matter Group, Department of Physics, King's College London, Strand Campus, London, UK
[b] INSERM, UMR-S665, DSIMB 75015, Universite Paris Diderot — Paris 7, UFR Life Sciences, Paris, France
[c] Randall Division of Cell and Molecular Biophysics, King's College London, New Hunt's House, Guy's Hospital, London, UK

ARTICLE INFO

Article history:
Received 10 July 2013
Received in revised form 29 October 2013
Accepted 3 December 2013
Available online 15 January 2014

Keywords:
Molecular dynamics simulation
HA fusion peptide
Lipid/peptide interaction
Coarse grained model

ABSTRACT

Membrane fusion is critical to eukaryotic cellular function and crucial to the entry of enveloped viruses such as influenza and human immunodeficiency virus. Influenza viral entry in the host cell is mediated by a 20–23 amino acid long sequence, called the fusion peptide. In the last years, possible structures for the fusion peptide and their implication in the membrane fusion initiation have been proposed; these ranging from an inverted V shaped α-helical structure to an α-helical hairpin, or to a complete α-helix. Here we develop a coarse grained approach to describe effectively the plasticity of the fusion peptide and the explored conformational states. We describe also a trimeric assembly for the fusion peptide and analyse the explored states in a 1-palmitoyl-2-oleoyl-*sn*-glycero-3-phosphocholine model membrane. For the single fusion peptide systems the kink angle observed experimentally for the V shaped structure shows a strong correlation with the orientation of the fusion peptide within the lipid bilayer. The trimeric fusion peptide model also experiences different conformational states and represents a more realistic model for the anchoring mechanism of one influenza haemagglutinin molecule. This article is part of a Special Issue entitled: Viral Membrane Proteins — Channels for Cellular Networking.

1. Introduction

It is well established that the surface glycoprotein covering the influenza viral capsid, influenza haemagglutinin (HA), is known to be responsible for binding to cells and the fusion of the viral and endosomal membranes [1–3]. HA is composed of three identical subunits and the N-terminal end of these subunits contains a sequence of ~20 N-terminal amino acids (**GLFGAIAGFI—ENGWEGMIDG**) that is called the fusion peptide (FP) [4]. During the viral infection process, a decrease in the local pH level provokes an extensive conformational rearrangement in each HA0, which unfurls the HA1 and HA2 chains [5]. As part of this unfurling process, the individual FPs are revealed and are inserted in the membrane of the healthy cell [6].

The mechanism and structure of the single FP as it inserts into the membrane of the healthy cell have been the focus of several experimental studies. Han and Tamm [7] have used circular dichroism (CD) spectroscopy and Attenuated Total Reflection (ATR)-Fourier Transform Infrared (FTIR) measurements to show that the FP adopt an *alpha*-helical structure upon inserting into model lipid membranes, which have a 4:1 molar ratio of 1-palmitoyl-2-oleoyl-*sn*-glycero-3-phosphocholine (POPC) to 1-palmitoyl-2-oleoyl-*sn*-glycero-3-phosphoglycerol (POPG). By combining the results of electron paramagnetic resonance (EPR), CD and NMR measurements, Han et al. also have proposed that FP inserted into dodecylphosphocholine (DPC) micelles and 4:1 POPC:POPG bilayers adopts an inverted 'V' structure [8], in which both the N- and C-terminal ends of the peptide are buried deeper into the membrane than the glycerol group and the 12ASN residue is closest to the fluid–membrane interface. Tamm proposed that influenza HA-mediated membrane fusion occurs via a spring-loaded boomerang mechanism, where the FP inserts into the target membrane and adopts a boomerang structure [9]. The boomerang structure is characterised by a kink angle within the inverted 'V' structure of ~120° [9], which is centred around the 12ASN residue [10,11].

Atomistic molecular dynamics simulations have also been used to attempt to gain a detailed description of the insertion of the influenza FP into model lipid membranes.

Lagüe et al. found that the equilibrium structure of the FP is more helical in POPC lipid membranes than in DPC micelles [12], which agrees well with the experimental findings of Han et al. [8]. The measured kink angle in the structure of the equilibrium configurations of the FP was

☆ This article is part of a Special Issue entitled: Viral Membrane Proteins — Channels for Cellular Networking.

* Corresponding authors.
E-mail addresses: franca.fraternali@kcl.ac.uk (F. Fraternali), chris.lorenz@kcl.ac.uk (C.D. Lorenz).

0005-2736/$ – see front matter © 2013 Published by Elsevier B.V.
http://dx.doi.org/10.1016/j.bbamem.2013.12.020

138° in the POPC bilayer, and 133° and 114° in DPC micelles made up of 32 and 56 lipids, respectively. Vaccaro et al. used the NMR structure found by Han et al. [8] as the starting configuration of the FP in their simulations, which showed that the first 11 residues of a FP monomer insert into a POPC bilayer as an α-helix at an angle of ~30° to the lipid/water interface and that it adopts an inverted V structure [13]. Huang et al. [14] and Panahi and Feig [15] also found that the FP monomer adopts a kinked structure, which is in good agreement with the NMR experiments of Han et al. [8], with the kink being located between residues 11GLU and 13GLY.

Molecular dynamics simulations of peptides at the interface with membrane have been studied recently with low resolution methods using implicit solvent models for the membranous environment [16–19].

In the near future all these approaches will be used efficiently in combination rather than in alternative, as one could effectively sample the orientation of proteins at the interface with the membrane, switch to a coarse grained model like the one presented here to refine and explore the possible assembling modes and conformational states, and finally accurately describe the interactions of the sampled stated by atomistic force fields. Recent NMR spectroscopy studies by Lorieau et al. report that the FP adopts a tight helical hairpin of two antiparallel α-helices at the lipid–fluid interface of DPC micelles, in which residue 13GLY has a positive dihedral angle that allows the FP to form the hairpin structure [20,21]. The inter-helical angle between the two helices is reported to be 158°, which infers that the kink angle is ~22°. The FP studied by Lorieau et al. contains three additional amino acid residues (21TRP, 22TYR and 23GLY) as compared to the FP strands studied in the previously discussed work. Residues 21TRP and 22TYR have been shown to help anchor proteins at the lipid–fluid interface [22,23], and the 23GLY can aid the stability of helices and interhelical interactions [24,25].

A very recent computational study [26] has investigated lipid tail protrusion to examine how fusion peptides might interact with membranes and promote fusion. Their atomistic simulations visit each of the states: kinked helix, straight helix, and a helical hairpin for the HA fusion peptide. In this manuscript, we developed a new coarse-grain model of the influenza FP monomer, which captures all the FP conformational states observed experimentally and computationally, and applied it to the study of the insertion of HA FP monomers and trimers into POPC lipid membranes. This model is used to study the behaviour of the wild type FP and a mutant FP, which contains a single mutation of the N-terminal residue from a glycine to a leucine, that has been shown experimentally to lower the fusion activity [27] and the replication rate of the virus [28]. For the monomeric systems the kink angle is found to show a strong dependence on the orientation of the FP within the lipid bilayer, which has not been reported previously.

In the trimeric systems, the correlation between the orientation of the FP and the kink angle of the FP is not as strong, however, preference for the FP monomers to adopt a helical hairpin structure is still observed. We discuss the results in the light of the mechanism of anchoring to the membrane of the entire HA molecule.

2. Simulation systems

Coarse-grain molecular dynamics simulations were conducted to study the evolution of the structure of the FP as it is inserted into a POPC bilayer. The wild type (**GLFGAIAGFI—ENGWEGMIDG**) and a mutant (**LLFGAIAGFI—ENGWEGMIDG**), which has a single mutation of the N-terminal residue from a glycine to a leucine, FPs have been studied to compare the difference in insertion behaviour.

The FP, lipids and water were modelled with the MARTINI coarse-grain force field [29,30]. An atomistic representation of the FP monomer was converted to the coarse-grain representation using the DSSP algorithm [31]. The MARTINI force field for proteins keeps the secondary structure of a protein rigid, therefore the force field for the FP was modified in order to allow the structure to change as it is inserted into the lipid bilayer. In doing so, the force constants for the dihedral angles that make up the backbone of residues 11GLU, 12ASN and 13GLY in the FP were modified in order to allow the peptide to find the two different kink angles observed experimentally (see Supporting Information for more details).

2.1. Monomer systems (system A)

In the monomer systems shown in Fig. 1, the FP monomer was placed with the N-terminal residue in the same plane as the PC headgroups of the POPC lipids in the bilayer, which consists of 36 lipids in each leaflet and has dimensions of 4.5 nm × 4.5 nm × 40 nm. Initially, the FP is tilted to an angle of ~40° with respect to the plane of the bilayer, which is in good agreement with previous experimental and computational studies [8,13,32–35].

2.2. Trimer systems (system B)

The assembled trimers were constructed by creating three replicas of the atomistic representation of the FP monomer modelled as a coiled coil FP trimer. The symmetry and orientation of the three helices are analogous to previous work on trimer assembly for these peptides [35]. This all-atom model was then transformed to a coarse-grain model assigning the secondary structure by the use of the DSSP algorithm [31]. In the HA molecule this coiled coil is attached to the rest of the molecule and therefore the peptides are not allowed to completely separate and diffuse within the membrane. Therefore, a constraint at the top of the trimer was added to closely represent this situation. An additional bead representing a GLY residue was added to the C-terminal end of each FP monomer, which was then used to connect the three monomers into a trimer by adding harmonic beads between these additional beads. In order to constrain the monomers into a trimeric structure representative of the atomistic model, the bonds between the additional GLY residues were modelled with a force constant of 5000 kJ mol^{-1} nm^{-2} and an equilibrium length of 1.1 nm and harmonic angle terms were added between the various additional GLY beads such that their equilibrium angle is 60°, and the force constant is 7000 kJ/(mol rad^2). These values for the bond and angle force constants are 4 and 10 times greater than the values used for the backbone beads of a peptide, respectively.

These assembled trimers of the wild type FP (system $\mathbf{B}_{wild}$) and mutant FP ($\mathbf{B}_{mutant}$) monomer were placed such that the N-terminal beads of each monomer in the trimer was lying in the same plane as the lipid head groups of a POPC bilayer with dimensions ~9.1 nm × 9.1 nm × 4.1 nm, which consists of 144 lipids in each leaflet (see Fig. 1).

3. Simulation methodology

A consistent simulation methodology was used in all simulations, including the monomer FP system for optimizing the value of the dihedral force constant. To equilibrate all the systems, a steepest descent energy minimisation was first carried out for 1000 steps. Three position restraint simulations were performed for each system after the energy minimisation in order to remove any overlapping beads that may still occur as a result of placing the trimers within the membrane. The position of the FP monomer/trimer was constrained by employing an initially high value of force constant (1000 kJ mol^{-1} nm^{-2}) in all directions for the first run. Each consecutive run employed a force constant decreased by an order of magnitude. For systems **B**, an additional short NVT simulation was performed at 300 K using a Nosé–Hoover thermostat [36,37] to keep the temperature constant.

The production run utilised the NPT ensemble, with a semi-isotropic Parrinello–Rahman [38] barostat to keep the pressure constant at 1.0 bar. A leap-frog integrator with a 20 fs timestep was used for all simulations. The van der Waals interactions were modelled via a shifted LJ potential with a 1.4 nm cut-off. Similarly, a shifted Coulomb potential

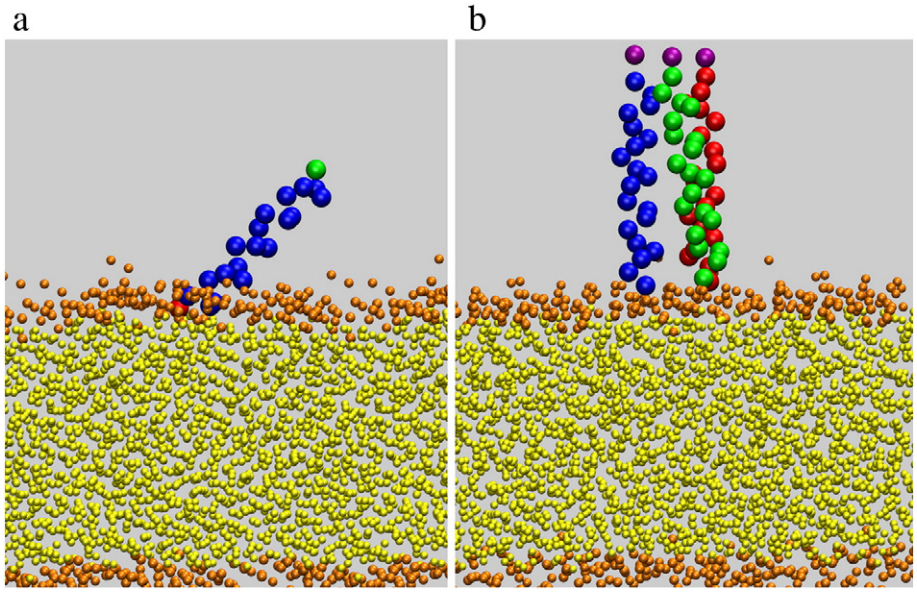

Fig. 1. Starting configurations used in the (a) monomer (system **A**) and (b) trimer (system **B**) simulations. In the picture of the monomer system, the backbone beads of the peptide are represented by blue spheres, with the N- and C-terminal beads shown in red and green, respectively. While in the snapshot of the trimer, the backbone beads of each monomer within the trimer are represented by blue, green and red spheres and the extra bead used to constrain the three monomers is the purple bead. The phosphate and choline groups of the lipid bilayer in both systems are shown as orange beads, with the glycerol group and the hydrocarbon tails shown as yellow spheres.

with a 1.2 nm cut-off was used to compute electrostatics. Each system ran for 500 ns, with trajectories written every 0.1 ns. The simulations were performed with GROMACS 4.5.3 [39].

Six replicas of systems $\mathbf{A}_{wild}$, $\mathbf{A}_{mutant}$, $\mathbf{B}_{wild}$ and $\mathbf{B}_{mutant}$ were run with different velocity seeds. In Section 1, the results of the replica systems are reported where sensible, and results from single trajectories which are representative of the behaviour observed in all of the replicas are used in order to show time dependent behaviour. Any discrepancies observed in the results of the various replicas will be discussed in the text.

4. Results and discussion

4.1. Simulation analysis

The trajectories from the production simulations from each replica of the systems were analysed so that a detailed understanding of the structure of the FP after insertion into the bilayer can be determined. In order to characterise the structure, the amount that each FP residue inserts into the POPC bilayer was determined, as was the kink and orientation angles for the FP after they have inserted into the bilayer. The results of the two monomer systems, $\mathbf{A}_{wild}$ and $\mathbf{A}_{mutant}$, allow the effects of a single residue mutation on these properties to be determined. While, the trimer systems were used to gain insight into how the structure of the monomers in a self-assembled structure similar to that found in the biological systems differ from that of the individual monomers.

In addition to the various measurements related to the insertion and structure of the FP, the main structural properties (for example area per lipid and order parameter) of the POPC lipid membrane have also been measured. However, there is no significant change in the membrane structure after the insertion of a monomer or a trimer, therefore these results have not been shown.

4.2. Insertion depth

The insertion depth of the monomer/trimer into the membrane is defined as the difference of the *z* coordinates of the backbone bead of each residue and the centre of mass of the phosphate and choline groups of the leaflet of the lipid bilayer with which the monomer/trimer

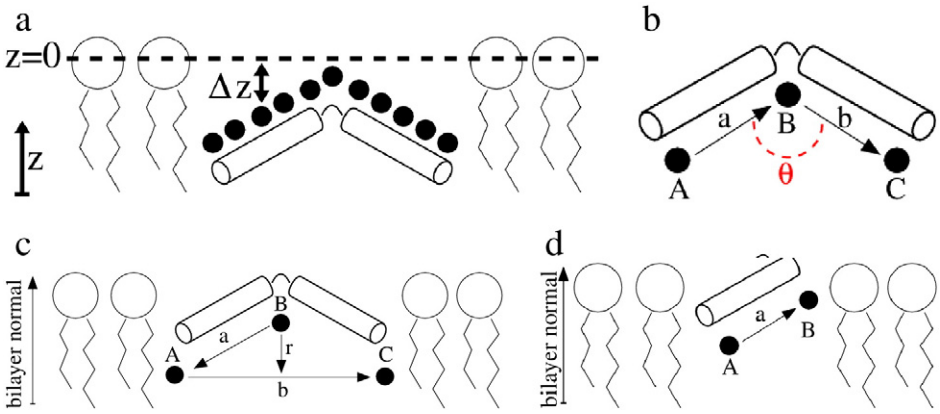

Fig. 2. Schematics of the definitions used for (a) insertion depth, (b) kink angle, (c) orientation angle and (d) tilt angle as they are calculated in this study.

is interacting, see Fig. 2a. A negative value indicates that the bead is inserted into the bilayer.

4.3. Kink (θ), orientation (ϕ) and tilt (ψ) angles

The kink, orientation and tilt angles of the peptide are important measures to characterise the structure and orientation of the peptide, once inserted into the membrane. Comparisons between the calculated kink angle and experimental observations [8–11,20,21] can be made. The orientation angle can also aid in deducing the structure of the peptide once inserted into the bilayer. Calculating the tilt angle also allows for comparisons to be made with experimental and computational studies [8,13,32–35].

The kink angle of the FP monomer is defined as the angle between the N-terminal, 12ASN and C-terminal residues, as depicted by beads **A**, **B** and **C** in Fig. 2b respectively. The kink angle is calculated at each timestep by Eq. (1).

$$\vec{a} \cdot \vec{b} = \left\|\vec{a}\right\| \left\|\vec{b}\right\| \cos(\theta) \tag{1}$$

where $\vec{a} = \left(\overrightarrow{AB}\right)$ and $\vec{b} = \left(\overrightarrow{BC}\right)$.

The orientation of the monomer with respect to the bilayer normal is calculated at each timestep, by first calculating the vector $\vec{r}$ Eq. (2), as depicted in Fig. 2c. The orientation angle is then calculated using Eq. (1), where $\vec{a} = \vec{r}$ and $\vec{b} = \vec{z} = (0\mathbf{i} + 0\mathbf{j} + \mathbf{k})$ (unit vector normal to the bilayer).

$$\vec{r} = \vec{a} - \vec{b}\left(\frac{\vec{a} \cdot \vec{b}}{\|\vec{b}\|^2}\right) \tag{2}$$

where $\vec{a} = \left(\overrightarrow{BA}\right)$ and $\vec{b} = \left(\overrightarrow{AC}\right)$.

The tilt angle is defined as the angle between the vector $\vec{a}$ and a unit vector normal to the membrane, $(\hat{z} = (0\mathbf{i} + 0\mathbf{j} + \mathbf{k}))$, as depicted in Fig. 2d. The tilt angle is determined by calculating the angle from Eq. (1) using $\vec{a}$ and $\vec{b} = \hat{z} = (0\mathbf{i} + 0\mathbf{j} + \mathbf{k})$, and then subtracting the angle from 90°. By calculating the difference between 90° and the measured angle, the angle between the peptide and the membrane is obtained.

By substituting the vectors $\vec{a}$ and $\hat{z}$ into Eq. (1), and subtracting the resulting angle from 90°, the tilt angle is obtained.

4.4. Monomer systems (system **A**)

4.4.1. Insertion depth

The insertion depth of the monomers in system **A** and the trimers in system **B** into the membrane is defined as the difference between the z coordinates (Δz) of the backbone bead of each residue and the centre of mass of the phosphate and choline groups of the lipid bilayer leaflet that is closest to the monomer/trimer. A negative value of Δz indicates that the given residue is inserted past the lipid headgroups into the bilayer. The insertion depth of each bead is averaged over the course of the trajectory during the entire production simulation, and the trajectories of each replica are averaged together.

Fig. 3 shows the average insertion depth of the backbone bead of each residue. A discernible trend in Fig. 3a is that the N-terminal residue of each monomer inserts 0.1–0.3 nm deeper into the membrane than the C-terminal glycine. The first three residues of the monomer in system $\mathbf{A}_{mutant}$ have inserted ~0.2 nm deeper into the membrane than those of the $\mathbf{A}_{wild}$ monomer, which is in contrast to the findings of Wu et al. [40]. This is due to the mutated residue 1LUE, which is hydrophobic, and is expected to have a greater insertion than 1GLY in the wild type monomer. The average insertion depths of the monomer in system $\mathbf{A}_{wild}$ (Fig. 3(a)) agree well with those observed experimentally [8,34]. Both studies found the insertion depth of 1GLY and 20GLY to be less than 0.5 nm, which is within the error (0.38 ± 0.11 nm for 1GLY and 0.30 ± 0.25 nm for 20GLY) of the calculated value for the same residues.

The average insertion depth of the monomers in system $\mathbf{A}_{wild}$ and $\mathbf{A}_{mutant}$ shows that the peptide is kinked. This can be seen in Fig. 3a (black and green dashed lines). The 1GLY and 20GLY of the wild type FP monomer have a greater insertion depth (~0.4 nm) than compared with the 12ASN residue (~0.1 nm), which is indicative of a kinked structure. The same can be said for the mutant FP monomer, however, the insertion depth of the 1LUE residue is 0.6 nm and the 20GLY is ~0.2 nm. Fig. 3b shows a representative snapshot of the $\mathbf{A}_{wild}$ monomer in a kinked structure.

The amphiphilic monomers contain mainly hydrophobic residues near the N-terminal end of the peptide, whilst the location of the kink has a charged (11GLU) and polar (12ASN) amino acid sequence. The hydrophobic residues are highlighted by the red boxes in the x-axis of Fig. 3a. The hydrophobic residues have inserted deeper into the membrane than the neutral and charged residues, as shown in Fig. 3a. Therefore, the ability to kink allows for the hydrophobic residues close

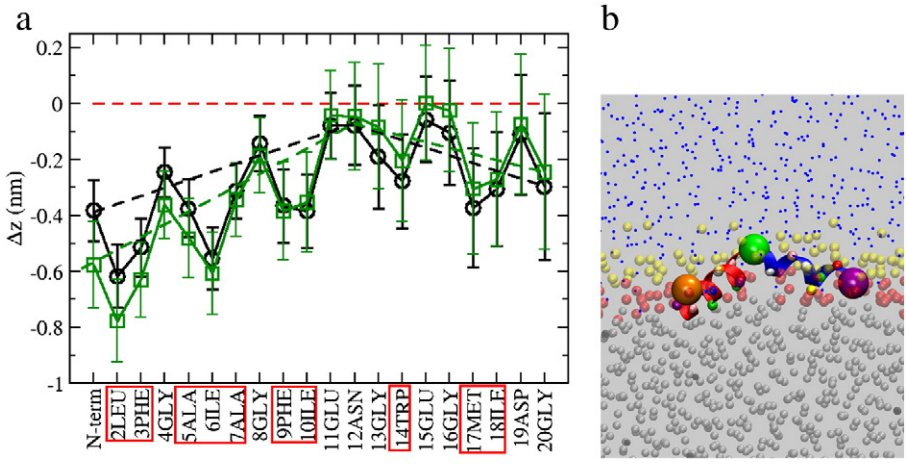

Fig. 3. (a) Average insertion depth of each residue in the wild type (black circles) and mutant (green squares) monomers in system **A**. The dashed red line represents the head groups of the bilayer leaflet closest to the monomer. The N-terminal is glycine for the wild type and leucine for the mutant, with the hydrophobic residues highlighted by red boxes. (b) Snapshots of system $\mathbf{A}_{wild}$ representing the insertion of the FP into the lipid membrane. The backbone beads of 1GLY, 12ASN and 20GLY residues are shown as large spheres coloured orange, green and purple respectively. The beads representing the PC head groups (yellow), glycerol group (red) and hydrocarbon tails (silver) of the lipid molecules and the water molecules (blue) have been reduced in size to make it easier to see the structure of the FP.

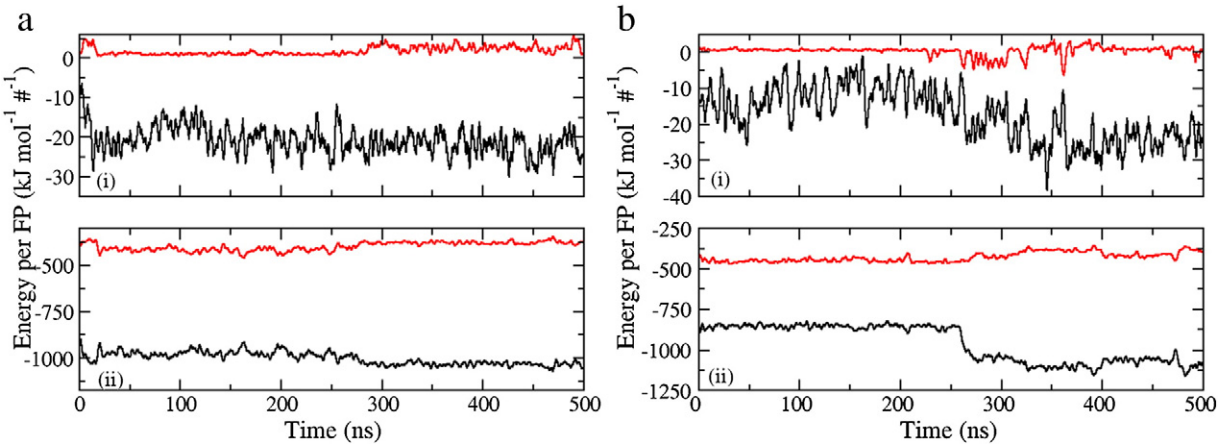

Fig. 4. The intermolecular (black) and intramolecular (red) contributions to the (i) electrostatic and (ii) van der Waals energy for systems (a) $\mathbf{A}_{wild}$ and (b) $\mathbf{A}_{mutant}$, respectively.

to the N-terminal to be inserted deeper, while the charged and polar groups are able to stay closer to the fluid–membrane interface and the oppositely charged lipid choline head groups. This can stabilise the monomer at the interface, and can be seen in the inverted 'V' structure proposed by Han et al. [8], where the N-terminal and C-terminal have larger insertion depths than the residues located at the kink angle (11GLU, 12ASN, and 13GLY), which is also observed in the simulations as shown in Fig. 3b.

The intermolecular (black line) and intramolecular (red line) electrostatic and van der Waals energy contributions are plotted as a function of time for systems $\mathbf{A}_{wild}$ and $\mathbf{A}_{mutant}$ in Fig. 4. In Fig. 4a and b, the intermolecular van der Waals energy profile shows a decrease, with the largest decrease in system $\mathbf{A}_{mutant}$, as the peptide inserts into the membrane. This decrease in energy shows that the peptide location at the interface is stable and the most energetically favourable. Any small increase in the intramolecular energies is offset by a larger decrease in the intermolecular energy in both systems, which shows that the overall net energy of the system is decreasing, or has stabilised.

Fig. 4b shows that as the peptide inserts into the membrane, there is a larger decrease in the intermolecular van der Waals energy, which stabilises to a similar value as that of the monomer in system $\mathbf{A}_{wild}$. An increase in the hydrophobic interactions between the FP and the membrane results in the decrease of the intermolecular van der Waals energy in both systems, and results in a small increase in the intramolecular van der Waals energy, as the peptide is able to obtain small kink angles. The peptide is able to obtain small kink angles at the interface, which increases the intramolecular interactions. In comparison to the change in the van der Waals energy, the change in the electrostatic energy of both systems $\mathbf{A}_{wild}$ and $\mathbf{A}_{mutant}$ is very small. The decrease observed in the electrostatic energy is mostly due to the negatively charged residues of the FP interacting with the choline groups of lipid headgroups.

Theoretical and experimental investigations of the conformational effects and free energy of association of influenza peptides to model membrane have been proposed in the past [41–43]. The interaction is shown to be driven by the enthalpy of peptide insertion in the bilayer and opposed by entropy loss due to the folding of the peptide in the membrane. As pointed out in these studies, the major folding event occurs at the N-terminal segment of the fusion peptide. Therefore accurate descriptions of the free energy events due to mutations at these positions are essential to understand the differences in fusogenic behaviour. Substitution of the C-terminal and highly conserved glycine residue with a serine or a valine has been demonstrated to have a dramatic effect on the NMR structure and CD spectra of this peptide in lipid bilayers and micelle environment. We can assume that similar effects would be observed for the G1L mutation studied here, if not enhanced. Nevertheless, systematic studies of all possible point mutations are still incomplete, both computationally and theoretically. The anisotropy of the media at the membrane interface and the crucial role of changes in pH render such studies difficult to realise.

4.5. Kink and orientation angles

Fig. 5 shows the calculated angles for the monomers in Systems $\mathbf{A}_{wild}$ and $\mathbf{A}_{mutant}$. The data shown in Fig. 5 is once the monomer has been inserted into the membrane, the visual inspection of the simulations for system $\mathbf{A}_{mutant}$ shows that the monomer inserts after 260 ns, while the monomer in system $\mathbf{A}_{wild}$ inserts from the start of the simulation.

For each timestep (that the peptide is inserted into the membrane), the orientation angle of the peptide within the membrane is plotted as a function of the peptide kink angle. From Fig. 5a and d, it is clear to see a correlation between the kink and orientation angles. The dependence of small kink to perpendicular orientation angles of the peptide (~90°, with respect to the membrane normal) and larger kink to higher orientation angles (>100°) is highlighted by the clustering of the data (red ellipses) in Fig. 5c and f.

The data in the insertion depth plots (Fig. 3a) show that the monomer resides at the fluid–membrane interface once it has been inserted. When the orientation of the peptide is perpendicular to the bilayer normal (~90°), the monomer has an acute kink angle (<60°). The C-terminal bead is generally less inserted into the bilayer in such helical hairpin structures. This conformation agrees well with experimentally observed structures of the FP by Lorieau et al. [20]. The orientation angle increases as the kink angle does, so for larger kink angle values, the orientation of the monomer is close to anti-parallel with the bilayer normal (~150°). Orientation angles greater than 90° can only exist if the N- and C-terminal beads are inserted deeper into the membrane than the 12ASN residue, supporting the inverted 'V' structure (boomerang) hypothesis [8]. Snapshots of the FP monomers in each of these two configurations are shown in Fig. 7.

In order to quantify the amount of time that a FP stays in a given conformation, the distribution of orientations and kink angles in Fig. 5c and f are used to label a given conformation as being in the hairpin orientation, inverted 'V' (boomerang) orientation or transitioning between the two. If the orientation angle is less than 120° and the kink angle is less than 110° then the FP is said to be in the hairpin configuration. Whereas if the orientation angle is greater than 120° and the kink angle is greater than 110° then the FP is labelled as being in the inverted 'V' (boomerang) configuration. Configurations in which the FP structure has any other pair of orientation and kink angles are said to be transitioning between the two structures.

Fig. 6a and b shows the probability distribution for a monomer in systems $\mathbf{A}_{wild}$ and $\mathbf{A}_{mutant}$, respectively, to be in the helical hairpin orientation, the inverted 'V' (boomerang) orientation, or transitioning between the two. Both monomers are more likely to be in the hairpin

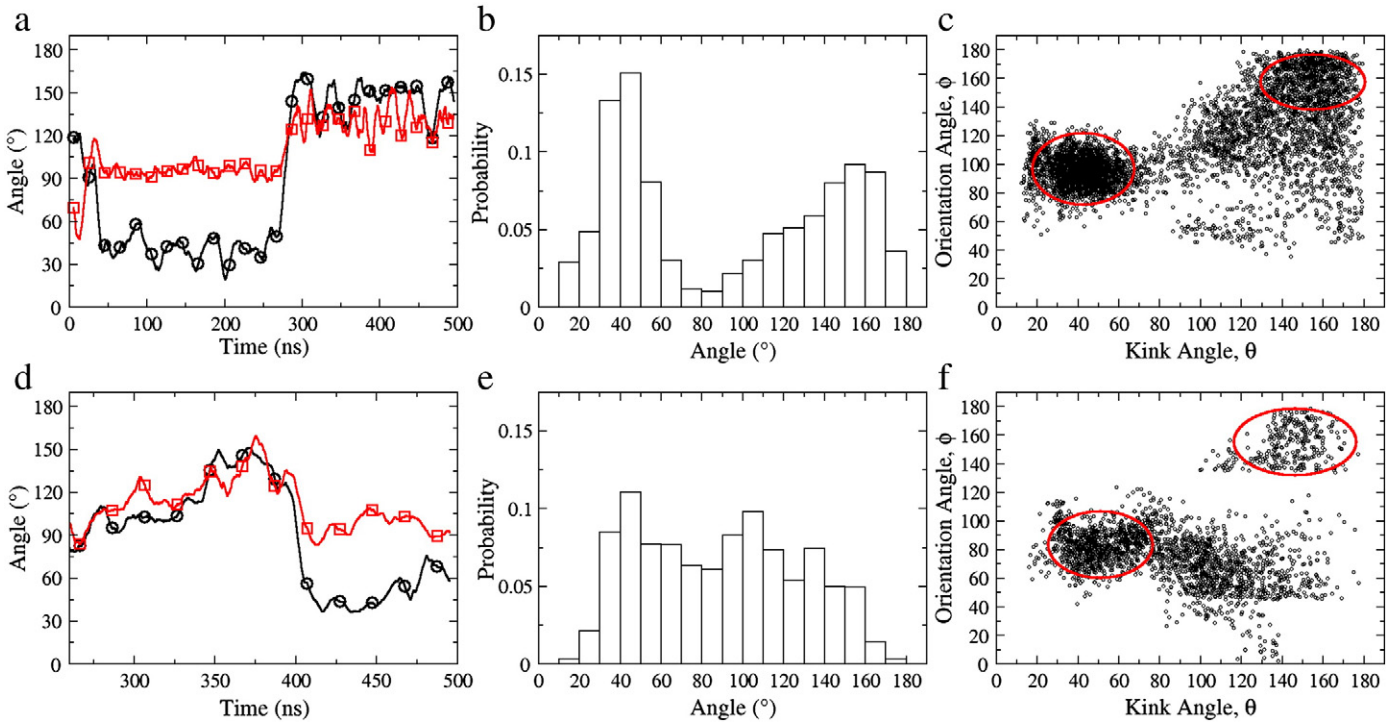

Fig. 5. Distribution of kink and orientation angles of system **A** simulations. (a & d) The kink (black) and orientation (red) angles of the wild type (a) and mutant (d) monomers in system **A** are plotted as a function of time (b & e) Histograms of the kink angles of the FP for the wild type (b) and mutant (e) monomers. (c & f) Plots of the orientation angle as a function of kink angle for the wild type (c) and mutant (f) monomers. The values of the two angles are calculated once the monomer has inserted into the membrane. The values plotted here are representative of a single replica; the other replicas which show similar behaviour can be found in the Supplementary Information.

orientation than the inverted 'V' and they both spend the least amount of time transitioning from one to the other. The wild type monomer has a higher probability to be in the hairpin orientation than the mutant monomer; while the mutant monomer is more likely to be in the inverted 'V' orientation than the wild type monomer. In any case, no matter which structure the single peptide would adopt, a mechanism by which a single FP could induce viral fusion is not directly reflecting the real situation. Single cell fusion studies are subject to the formation of fusion pores, as early intermediates in the fusion process. Some models suggest up to six HA trimers participating in the formation of a single pore. It is possible that during the process of pore formation the peptide rearranges from the possible states of helical hairpin or boomerang orientation to a contiguous α-helical state effective to the formation of such oligomeric pores.

The tilt angle of the monomers upon insertion is in the range of 25°–40° (not shown), which is in very good agreement with experimental and computational results [8,13,32–35], which report values between 23° and 40°. The tilt angle also stabilises within the first 10 ns, which has also been observed in other simulations [13,35]. Simulations of monomers initially oriented perpendicular to the lipid interface with the N-terminal end closest to the membrane as well as monomers oriented such that the C-terminal residue of the FP was nearest the lipid interface were also conducted. In all cases, the peptide did not insert until the N-terminal residue of the FP was nearest in the interface and the monomer made a tilt angle in the stated range with the lipid interface. There is a discernible trend in the intermolecular energies with respect to the kink angle, such that an increase in the kink angle of the peptide results in an increase in the intramolecular van der Waals energy. A 120° increase in the kink angle for the monomer in both systems $\mathbf{A}_{wild}$ and $\mathbf{A}_{mutant}$ results in an increase of ~50 kJ mol^{-1} in the intramolecular van der Waals energy. An increase in the kink angle, which causes the distance between the N- and C-terminals of the peptide to increase, causes the intramolecular energy to increase. However, the changing configuration of the peptide (increase in kink angle) subsequently causes the intermolecular van der Waals energy to decrease, as the interactions between the hydrophobic residues and the bilayer increase. A highly kinked configuration of the peptide (with small kink angles ~30°) is at a lower intramolecular

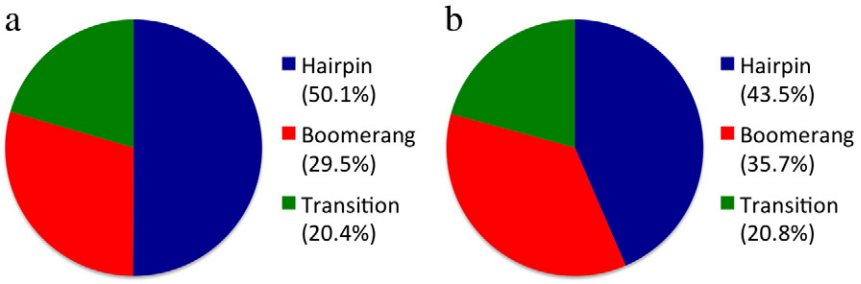

Fig. 6. Probability distribution that a monomer in system (a) $\mathbf{A}_{wild}$ and (b) $\mathbf{A}_{mutant}$ is in the helical hairpin orientation (blue), the inverted 'V' or boomerang orientation (red) or transition between the two (green).

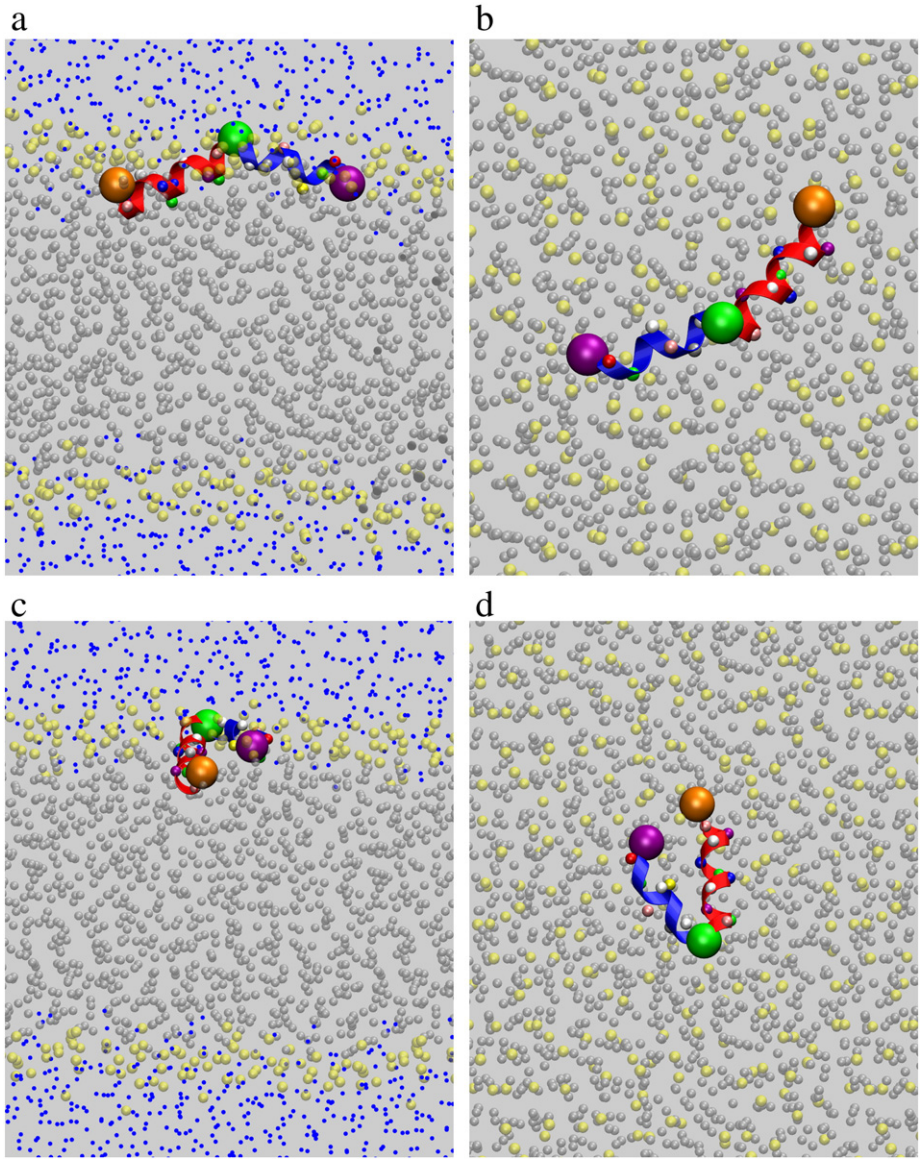

Fig. 7. Snapshots showing the kink and orientation angle for the monomer in system $\mathbf{A}_{wild}$. The kink and orientation angles for (a) and (b) are 126.00° and 136.65° respectively. The kink and orientation angles for (c) and (d) are 27.70° and 98.79° respectively. The N-terminal, 12ASN and C-terminal beads are shown as orange, green and purple spheres. The red and blue α-helices are between the N-terminal and 12ASN and 12ASN and C-terminal of each monomer respectively. The phosphate and choline, hydrocarbon tails and water are represented as yellow, silver and blue spheres respectively.

energy (~−425 kJ mol^{-1}), as the hydrophobic residues are closer together. The intermolecular van der Waals energy decreases by the same amount.

*4.6. Trimer systems (system **B**)*

4.6.1. Insertion depth

The insertion depth profiles of the wild type trimer in systems $\mathbf{B}_{wild}$ are considerably different to those of the monomers in system **A**. Fig. 8 shows the average insertion depths of each residue for each monomer within the trimer. The average location of the C-terminal beads of the trimer is ~0.80 nm away from the phosphate and choline groups (outside of the membrane), which has a difference of ~1.00 nm to the monomers in system **A**, as the extra beads used to self assemble the monomers into a trimer prevent the C-terminal beads from penetrating the bilayer. The C-terminal beads of the monomers in system **A** have no such restriction placed on them, and therefore can penetrate into the bilayer. Fig. 8 shows that the first ten residues (from 1GLY to 10ILE) of each monomer prefers to be inserted, while the peptide segment from 13GLY to 20GLY resides at the fluid–membrane interface due to the polar and charged residues.

The insertion of wild type monomers and trimers is consistent with a computational study of FP monomers and trimers inserted into bilayers by Sammalkorpi and Lazaridis [35]. It was observed that wild type FP monomers inserted into a bilayer with varied depths, always diffused to the interface, with a tilted configuration, which is seen in Fig. 3a. The monomers within a trimer also relocated to the interface, with one or more monomers inserted into the membrane, which is consistent with Fig. 8a.

The N-terminal residue in the mutant trimer (1LEU) does not penetrate the membrane by more than 1.5 nm, which is the same maximum depth for the N-terminal residue in the wild type trimer (1GLY). The average position of each monomer indicates the trimer resides at the interface, which is expected. The first three residues of the monomers in the mutant trimer insert ~0.2 nm deeper than their counterparts in the monomers of the wild type trimers, which is similar to the difference observed in the monomer system **A**.

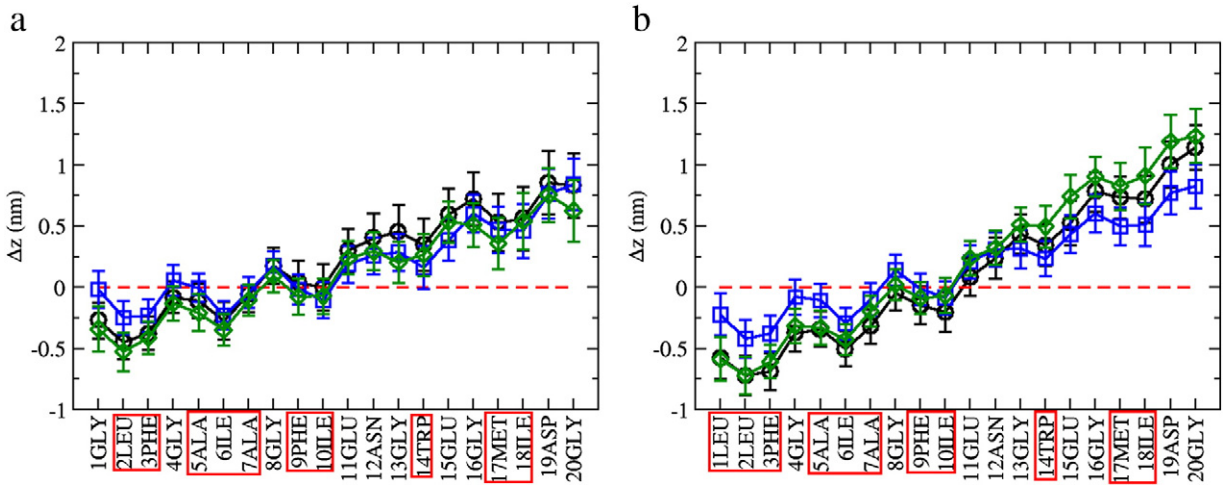

Fig. 8. Average insertion depth of each residue of the different monomers (represented by black circles, green squares and blue diamonds) of the trimer made up of (a) wild type monomers ($\mathbf{B}_{wild}$) and of (b) mutant monomers ($\mathbf{B}_{mutant}$). The dashed red line represents the head groups of the bilayer leaflet closest to the monomer. The N-terminal is glycine for the wild type and leucine for the mutant, with the hydrophobic residues highlighted by red boxes.

Fig. 9 shows the intermolecular and intramolecular contributions to the van der Waals and electrostatic energies of the trimer systems. The intermolecular (black line) van der Waals energy decreases for system $\mathbf{B}_{wild\text{-}head}$. This is in agreement with the behaviour of the monomers in system **A**, as the value of the intermolecular van der Waals energy is at its lowest when the monomer/trimer is located at the interface. The energetically favourable state for each monomer of the trimer in system **B** is at the membrane–fluid interface. Therefore, it is the van der Waals interactions which are driving the trimer to the interface as opposed to a Coulombic interaction.

Surprisingly, there is an increase in the intermolecular van der Waals energy in system $\mathbf{B}_{mutant\text{-}head}$, however, this is offset by the decrease in the intramolecular energy. This shows that the intramolecular van der Waals energy decreases as each monomer of the trimer spreads out and reaches the interface, with the increase in the intermolecular van der Waals energy attributed to an increased interaction between each monomer and the environment. The intermolecular and intramolecular electrostatic energies within system **B** fluctuate around -20 kJ mol^{-1} and 0 kJ mol^{-1} respectively, which is also observed for system **A**. The van der Waals and electrostatic energies were calculated for the whole trimer as opposed to calculating the energies for each individual trimer, during the simulations. Therefore, it is not possible to determine any correlations between the interpeptide distance and the inter- and intramolecular energies.

The kink, orientation and tilt angles were calculated for each individual monomer self assembled into the trimer in system **B**, in the same way as for the monomer in system **A**. The results for each peptide are shown in Fig. 10.

From Fig. 10a and c, it can be seen that one of the monomers has a kink angle ~80° for the majority of the simulation, whilst the other two of the three monomers of the trimer in system $\mathbf{B}_{wild}$ do not exhibit acute kink angles (<60°). From the average insertion depths of each monomer (Fig. 8a), it can be seen that the N-terminal ends of two monomers are slightly more inserted than the third. The two that are inserted more also are found to be the two monomers which have larger kink angles. This implies that the structure of the trimer is such that on average, all three monomers are located at the fluid–membrane interface, however, the greater average insertion (of the residues close to the N-terminal) of the two monomers prevents a smaller kink angle. A representative snapshot of a trimer in which the above is exhibited is shown in Fig. 11. The orientation angle of each monomer does not exhibit the same behaviour as that of the monomers in system $\mathbf{A}_{wild}$ (Fig. 5a and c).

Fig. 12a and b shows the probability distribution that the monomers that make up the trimers in system $\mathbf{B}_{wild}$ and $\mathbf{B}_{mutant}$, respectively, are in the helical hairpin orientation, inverted 'V' orientation or transitioning between the two. In both systems, monomers are most likely to be found in the helical hairpin orientation, which is similar to the trend

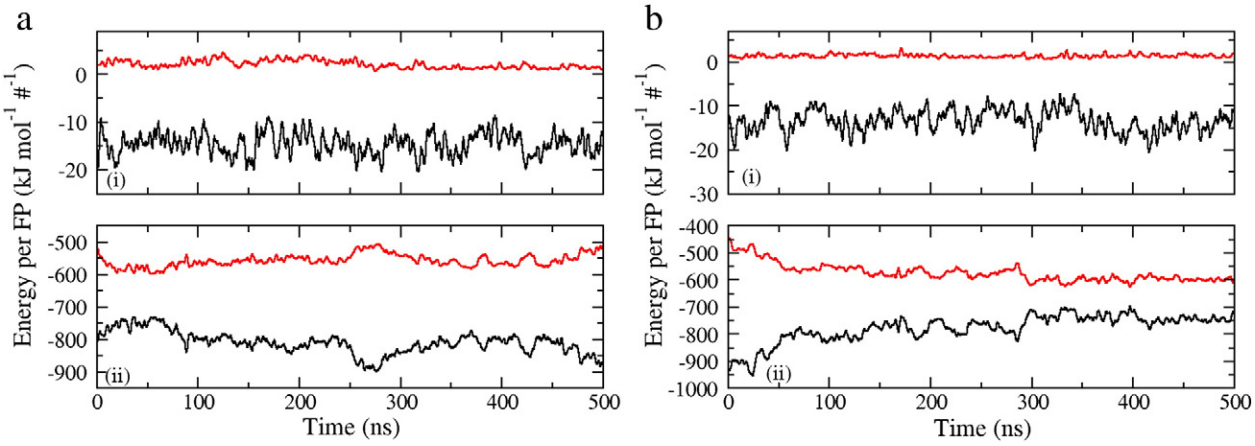

Fig. 9. The intermolecular (black) and intramolecular (red) contributions to the (i) electrostatic and (ii) van der Waals energy for systems (a) $\mathbf{B}_{wild}$ and (b) $\mathbf{B}_{mutant}$, respectively.

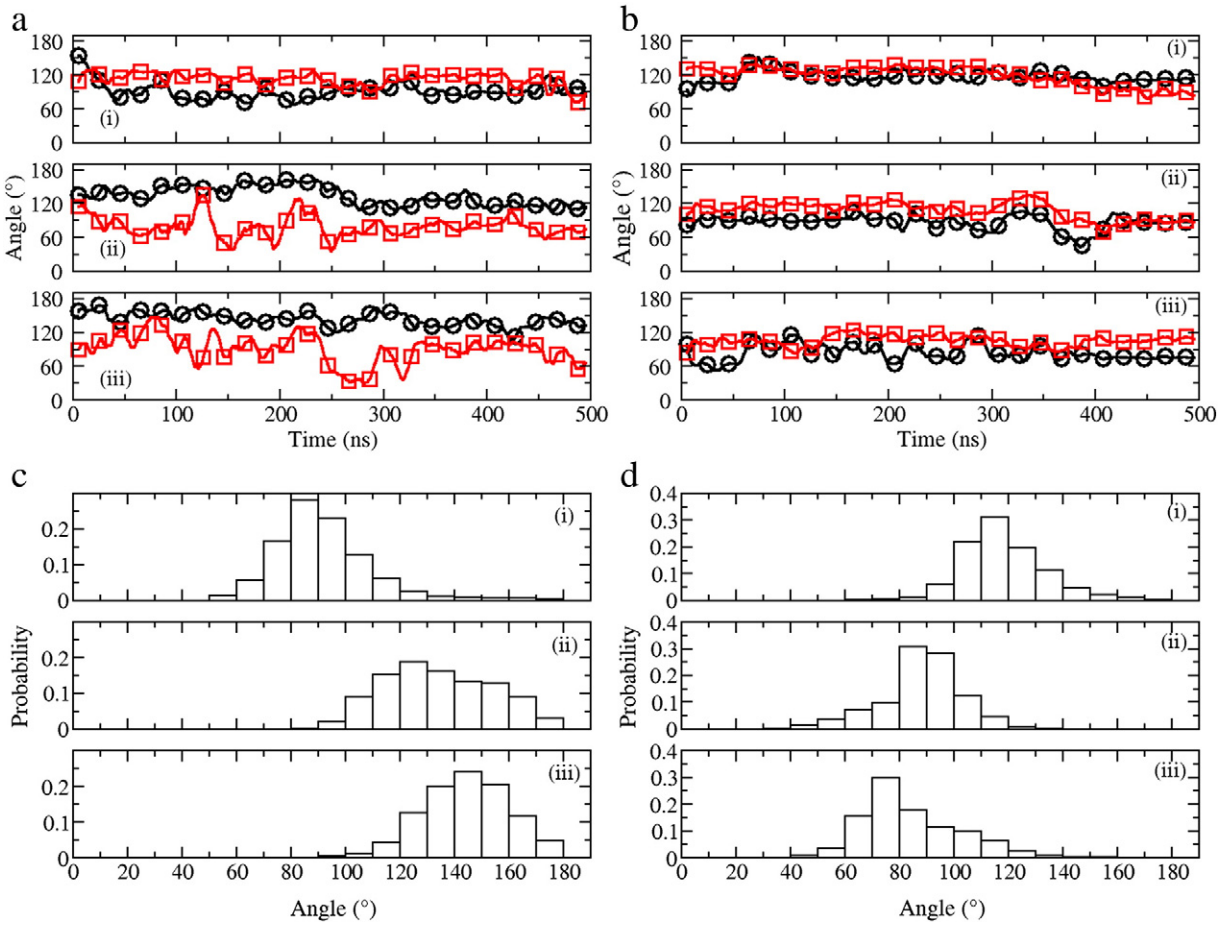

Fig. 10. The kink (black) and orientation (red) angles of the trimer in system $\mathbf{B}_{wild}$ (only one replica simulation data shown).

found in the monomer systems. However, in the trimer systems, the probability that the monomers are found in the helical hairpin orientation is significantly larger than that of the monomer systems and the probability that they are found in the inverted 'V' (boomerang) orientation is about a third of that for the monomer systems. Also, in this case the mutant monomers have a higher probability of being in the hairpin orientation than the wild type monomers, which is the opposite of what was observed for the monomer systems (system **A**).

This is in contrast to the trimer in system $\mathbf{B}_{mutant}$ (Fig. 10b and d), where each of the monomers within the trimer have similar kink angles. The average insertion depths (Fig. 8b) are also very similar for each monomer, which implies that the structure of the trimer within the

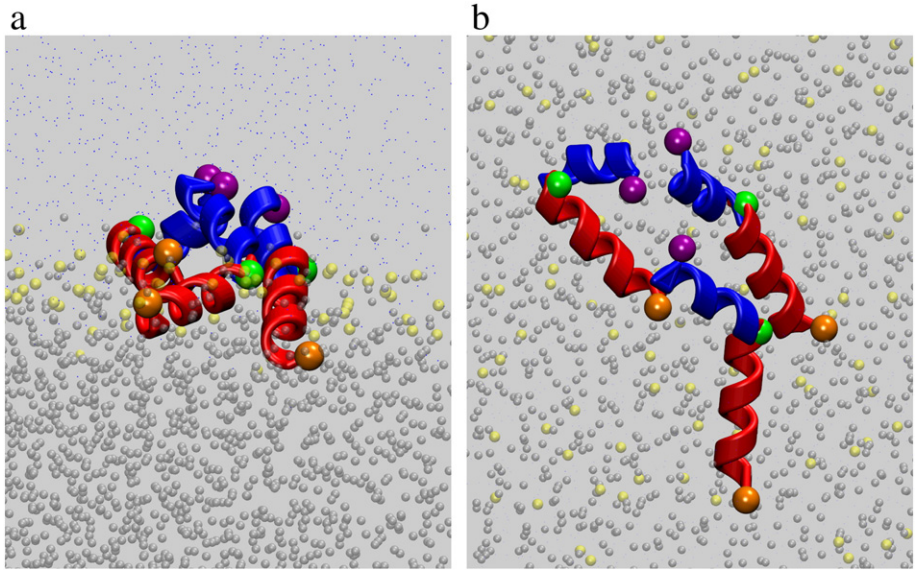

Fig. 11. Snapshots of an inserted configuration of the monomers in the trimer in system $\mathbf{B}_{wild}$ (a) side view, (b) top view. Each monomer is represented by a blue and red helix which connect the C-terminal (purple sphere) and 12ASN (green sphere) and the 12ASN and the N-terminal (orange spheres) residues, respectively. The lipid head groups, lipid tails and water beads are represented by yellow, silver and blue spheres, respectively, and the size of these spheres have been reduced such that the structure of the monomers is clearly observed.

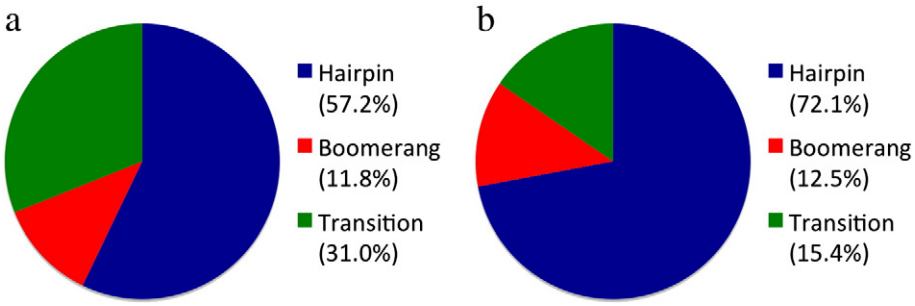

Fig. 12. Probability distribution that a monomer in system (a) $\mathbf{B}_{wild}$ and (b) $\mathbf{B}_{mutant}$ is in the helical hairpin orientation (blue), the inverted 'V' or boomerang orientation (red) or transition between the two (green).

bilayer is such that the N-terminal residues are inserted deeper into the membrane than the C-terminal residues.

The monomers which are self assembled into a trimer do not exhibit the smaller kink angles (<50°) as observed in the single monomers in system **A**. We believe this is due to the additional beads and bonded restraints on the C-terminal beads, which keep them from inserting as deeply into the bilayer as when they are completely free to move. For the small kink angles observed in system **A**, the insertion depths of the N- and C-terminal beads were similar.

The orientation angles for the monomers self-assembled into trimers are in agreement with the observed trend between the insertion depth and the orientation angles of the monomers in system **A**. In system **A**, when the C-terminus of the monomer is less inserted than the N-terminus, the measured orientation angles were always greater than 100°, which is consistent with the values of the orientation angles measured in the monomers that make up the trimers in system **B**.

The tilt angles of each monomer in the trimer have been measured (not shown), with the average tilt angle for systems $\mathbf{B}_{wild}$ and $\mathbf{B}_{mutant}$, 20.1° ± 7.5° and 24.2° ± 5.6° respectively. These values are also in good agreement with experimental and computational studies [8,13,32–35]. The value of the tilt angle stabilises very quickly and remains nearly constant at ~30°, which is the same value observed for the monomers in system **A**.

In conclusion, we believe that the peculiar plasticity of the FP sequence is needed for adaptation to the different environments that the peptide has to experience during membrane fusion. Additionally, flexibility to adopt all the states observed experimentally and computationally (inverted 'V' helix, helix–hairpin and all-helix) is necessary for the formation of oligomeric pores that create narrow aqueous channels as pre-fusion states [26]. Our model for trimers assembly can be considered as a first step towards a more realistic description of the effective mechanisms playing a role in the early intermediate states of the fusion process.

Additionally we believe the approach presented here of modifying the existing MARTINI force field in order to reproduce structures observed from experimental measurements and/or atomistic molecular dynamics simulations is one that could generally be applied to the general field of peptides interacting with interfaces. In this manuscript, the method has been applied to a small peptide which only had one significant change in the configuration observed. When studying larger peptides and proteins, the task of accurately capturing the configurational changes of the peptide as it interacts with the interface will prove more challenging, as not only will one need to accurately reproduce the structural changes but also do so in the correct sequence. However, we believe that this approach is a good starting point for attempting to model these more challenging problems. If one takes a sequential approach to capturing the various changes in the peptide's structural conformation, this approach could provide a new insight into the underlying physics which control the sequence of the conformational changes that a peptide undergoes while interacting with an interface.

Appendix A. Supplementary data

Supplementary data to this article can be found online at http://dx.doi.org/10.1016/j.bbamem.2013.12.020.

References

[1] D.C. Wiley, J.J. Skehel, The structure and function of the hemagglutinin membrane glycoprotein of influenza virus, Annu. Rev. Biochem. 56 (1987) 365–394.
[2] J.J. Skehel, D.C. Wiley, Receptor binding and membrane fusion in virus entry: the influenza hemagglutinin, Annu. Rev. Biochem. 69 (2000) 531–569.
[3] J.J. Skehel, K. Cross, D. Steinhauer, D.C. Wiley, Influenza fusion peptides, Biochem. Soc. Trans. 29 (2001) 623–626.
[4] F.S. Cohen, G.B. Melikyan, Implications of a fusion peptide structure, Nat. Struct. Mol. Biol. 8 (2001) 653–655.
[5] P. Durrer, C. Galli, S. Hoenke, C. Corti, R. Glück, T. Vorherr, J. Brunner, H^+-induced membrane insertion of influenza virus hemagglutinin involves the HA2 amino-terminal fusion peptide but not the coiled coil region, J. Biol. Chem. 271 (1996) 13417–13421.
[6] C.M. Carr, C. Chaudhry, P.S. Kim, Influenza hemagglutinin is spring-loaded by a metastable native conformation, Proc. Natl. Acad. Sci. 94 (1997) 14306–14313.
[7] X. Han, L.K. Tamm, A host–guest system to study structure–function relationships of membrane fusion peptides, Proc. Natl. Acad. Sci. 97 (2000) 13097–13102.
[8] X. Han, J.H. Bushweller, D.S. Cafiso, L.K. Tamm, Membrane structure and fusion-triggering conformational change of the fusion domain from influenza hemagglutinin, Nat. Struct. Mol. Biol. 8 (2001) 715–720.
[9] L.K. Tamm, Hypothesis: spring-loaded boomerang mechanism of influenza hemagglutinin-mediated membrane fusion, Biochimica et Biophysica Acta (BBA) — Biomembranes 1614 (2003) 14–23.
[10] L.K. Tamm, F. Abildgaard, A. Arora, H. Blad, J.H. Bushweller, Structure, dynamics and function of the outer membrane protein A (OmpA) and influenza hemagglutinin fusion domain in detergent micelles by solution NMR, FEBS Lett. 555 (2003) 139–143.
[11] A.L. Lai, L.K. Tamm, Locking the kink in the influenza hemagglutinin fusion domain structure, J. Biol. Chem. 282 (2007) 23946–23956.
[12] P. Lagüe, B. Roux, R.W. Pastor, Molecular dynamics simulations of the influenza hemagglutinin fusion peptide in micelles and bilayers: conformational analysis of peptide and lipids, J. Mol. Biol. 354 (2005) 1129–1141.
[13] L. Vaccaro, K.J. Cross, J. Kleinjung, S.K. Straus, D.J. Thomas, J.J. Wharton, S.A. Skehel, F. Fraternali, Plasticity of influenza haemagglutinin fusion peptides and their interaction with lipid bilayers, Biophys. J. 88 (2005) 25–36.
[14] Q. Huang, C.L. Chen, A. Herrmann, Bilayer conformation of fusion peptide of influenza virus hemagglutinin: a molecular dynamics simulation study, Biophys. J. 87 (2004) 14–22.
[15] A. Panahi, M. Feig, Conformational sampling of influenza fusion peptide in membrane bilayers as a function of termini and protonation states, J. Phys. Chem. B 114 (2010) 1407–1416.
[16] D. Bechor, N. Ben-Tal, Implicit solvent model studies of the interactions of the influenza hemagglutinin fusion peptide with lipid bilayers, Biophys. J. 80 (2001) 643–655.
[17] T. Lazaridis, Effective energy function for proteins in lipid membranes, Proteins Struct. Funct. Bioinf. 52 (2003) 176–192.
[18] W. Im, M. Feig, C.L. Brooks, An implicit membrane generalized born theory for the study of structure, stability, and interactions of membrane proteins, Biophys. J. 85 (2003) 2900–2918.
[19] S. Tanizaki, M. Feig, A generalized Born formalism for heterogeneous dielectric environments: application to the implicit modeling of biological membranes, J. Chem. Phys. 122 (2005) 124706.
[20] J.J. Lorieau, J.M. Louis, A. Bax, The complete influenza hemagglutinin fusion domain adopts a tight helical hairpin arrangement at the lipid:water interface, Proc. Natl. Acad. Sci. 107 (2010) 11341–11346.
[21] J.L. Lorieau, J.M. Louis, A. Bax, Helical hairpin structure of influenza hemagglutinin fusion peptide stabilized by charge–dipole interactions between the N-terminal amino group and the second helix, J. Am. Chem. Soc. 133 (2011) 2824–2827.

[22] M. Schiffer, C.-H. Chang, F. Stevens, The function of tryptophan residues in membrane proteins, Protein Eng. 5 (1992) 213–214.
[23] D. Stopar, R.B. Spruijt, M.A. Hemminga, Anchoring mechanisms of membrane-associated M13 major coat protein, Chem. Phys. Lipids 141 (2006) 83–93.
[24] W.P. Russ, D.M. Engelman, The GxxxG motif: a framework for transmembrane helix–helix association, J. Mol. Biol. 296 (2000) 911–919.
[25] G. Kleiger, R. Grothe, P. Mallick, D. Eisenberg, GXXXG and AXXXA: common alpha-helical interaction motifs in proteins, particularly in extremophiles, Biochemistry 41 (2002) 5990–5997.
[26] P. Larsson, P.M. Kasson, Lipid tail protrusion in simulations predicts fusogenic activity of influenza fusion peptide mutants and conformational models, PLoS Comput. Biol. 9 (2013) e1002950.
[27] D.A. Steinhauer, S.A. Wharton, J.J. Skehel, D.C. Wiley, Studies of the membrane fusion activities of fusion peptide mutants of influenza virus hemagglutinin, J. Virol. 69 (1995) 6643–6651.
[28] K.J. Cross, S.A. Wharton, J.J. Skehel, D.C. Wiley, D.A. Steinhauer, Studies on influenza haemagglutinin fusion peptide mutants generated by reverse genetics, EMBO J. 20 (2001) 4432–4442.
[29] S.J. Marrink, H.J. Risselada, S. Yefimov, D.P. Tieleman, A.H. de Vries, The martini force field: coarse grained model for biomolecular simulations, J. Phys. Chem. B 111 (2007) 7812–7824.
[30] L. Monticelli, S.K. Kandasamy, X. Periole, R.G. Larson, D.P. Tieleman, S.J. Marrink, The MARTINI coarse-grained force field: extension to proteins, J. Chem. Theory Comput. 4 (2008) 819–834.
[31] W. Kabsch, C. Sander, Dictionary of protein secondary structure: pattern recognition of hydrogen-bonded and geometrical features, Biopolymers 22 (1983) 2577–2637.
[32] J.C. Macosko, C. Kim, Y. Shin, The membrane topology of the fusion peptide region of influenza hemagglutinin determined by spin-labeling EPR, J. Mol. Biol. 267 (1997) 1139–1148.
[33] J. Lüneberg, I. Martin, F. Nüssler, J.M. Ruysschaert, A. Herrmann, Structure and topology of the influenza virus fusion peptide in lipid bilayers, J. Biol. Chem. 270 (1995) 27606–27614.
[34] Z. Zhou, J.C. Macosko, D.W. Hughes, B.G. Sayer, J. Hawes, R.M. Epand, ^{15}N NMR study of the ionization properties of the influenza virus fusion peptide in zwitterionic phospholipid dispersions, Biophys. J. 78 (2000) 2418–2425.
[35] M. Sammalkorpi, T. Lazaridis, Configuration of influenza hemagglutinin fusion peptide monomers and oligomers in membranes, Biochimica et Biophysica Acta (BBA) — Biomembranes 1768 (2007) 30–38.
[36] S. Nos, A molecular dynamics method for simulations in the canonical ensemble, Mol. Phys. 52 (1984) 255–268.
[37] W.G. Hoover, Canonical dynamics: equilibrium phase-space distributions, Phys. Rev. A 31 (1985) 1695–1697.
[38] M. Parrinello, A. Rahman, Polymorphic transitions in single crystals: a new molecular dynamics method, J. Appl. Phys. 52 (1981) 7182–7190.
[39] B. Hess, C. Kutzner, D. van der Spoel, E. Lindahl, GROMACS 4: algorithms for highly efficient, load-balanced, and scalable molecular simulation, J. Chem. Theory Comput. 4 (2008) 435–447.
[40] C.W. Wu, S.F. Cheng, W.N. Huang, V.D. Trivedi, B. Veeramuthu, B.K. Assen, W.G. Wu, D.K. Chang, Effects of alterations of the amino-terminal glycine of influenza hemagglutinin fusion peptide on its structure, organization and membrane interactions, Biochimica et Biophysica Acta (BBA) — Biomembranes 1612 (2003) 41–51.
[41] Y. Li, X. Han, Thermodynamics of fusion peptide-membrane interactions, Biochemistry 42 (2003) 7245–7251.
[42] J. Li, P. Das, R. Zhou, Single mutation effects on conformational change and membrane deformation of influenza hemagglutinin fusion peptides, J. Phys. Chem. B 114 (2010) 8799–8806.
[43] M. Haque, H. Chakraborty, T. Koklic, H. Komatsu, Hemagglutinin fusion peptide mutants in model membranes: structural properties, membrane physical properties, and PEG-mediated fusion, Biophys. J. 101 (2011) 1095–1104.